Journal of Applied Fluid Mechanics, Vol. 18, No. 5, pp. 1174-1188, 2025.
Available online at www.jafmonline.net, ISSN 1735-3572, EISSN 1735-3645.
https://doi.org/10.47176/jafm.18.5.3177

Enhancement of Savonius Wind Turbine Performance Through Blade Optimization

O. Hazar, M. Dirgenali, K. Kaçar and S. Elçi†

Izmir Institute of Technology, Izmir, Urla, 35430, Turkey

†*Corresponding Author Email: sebnemelci@iyte.edu.tr*

ABSTRACT

The objective of this study is to create an innovative blade design that enhances the power efficiency of the Savonius rotors. This is achieved by optimizing the blade shape of the traditional Savonius rotor using the ANSYS Adjoint solver program. The results of the analysis revealed that the total pressure exerted on the optimized shape was 16 times greater than that of the traditional Savonius rotor. To compare performance metrics, the rotor with the optimized blade structure was numerically modeled alongside the traditional and Banesh-type Savonius rotors using the ANSYS Fluent program. The Dynamic Mesh 6DOF method is used in the model domain in order to simulate rotation of the rotor. The rotors were then analyzed in two different configurations: as a single-stage rotor with a phase angle of 0°, and as a three-stage rotor with a phase angle of 60° between each stage while keeping rotor height constant. The optimized blade rotor with 3 stages demonstrated superior performance with a power coefficient of 0.44, outperforming both the Banesh and traditional Savonius rotors, while also displaying power coefficient values 18.9% and 37.5% higher than the Banesh-type Savonius and traditional Savonius rotors, respectively.

Article History

Received October 5, 2024
Revised December 8, 2024
Accepted December 30, 2024
Available online March 4, 2025

Keywords:

Optimized rotor blades
Ansys Fluent
Dynamic mesh
Ansys adjoint solver
Power coefficient

1. INTRODUCTION

Advancements in technology, coupled with a growing global population, have escalated the demand for energy like never before. This surge in energy consumption has led to an increased demand on fossil fuels, resulting in a significant rise in emissions that damage the global ecosystem. Wind energy, however, presents a safer and cleaner alternative. In the face of global climate change and the need for sustainability, investments in renewable energy sources, such as wind energy, are on the rise worldwide. According to IRENA (2019) wind energy has the potential to supply 35% of the world's power demand as a leading source of global energy. However, in the same report it is also noted that in order to achieve this goal total installed wind capacity worldwide needs to reach 6,000 gigawatts by 2050 which is tenfold of the current installed capacity. According to the IEA (2024), wind energy holds immense potential to boost the growth of renewable capacity in countries worldwide. The projections for solar and wind energy additions suggest a more than twofold increase by 2028, compared to the levels in 2022. The Global Wind Atlas was launched by the World Bank and the Technical University of Denmark in order to assist investors in pinpointing potential locations for wind power generation across the globe. Wind energy's role is becoming more critical with each passing day, as demonstrated by this event and others like it. Simultaneously, there's a growing trend and an increase in incentives that encourage the use of wind energy.

Wind turbines can be classified as vertical axis wind turbine (VAWT) and horizontal axis wind turbine (HAWT). A Savonius wind turbine is a type of vertical-axis wind turbine (VAWT) that converts the force of the wind into torque on a rotating shaft. The Savonius rotor was invented by Finnish engineer Sigurd Johannes Savonius in 1922 (Giovanni, 2019). Beyond their primary role in electrical power generation, Savonius rotors find diverse applications. They can be utilized for water pumping and lake aeration, enhancing water quality and circulation. The turbine consists of two or more half-cylindrical blades, usually mounted on a vertical shaft or framework. The blades are curved to create a differential drag when exposed to the wind, causing the turbine to spin. Savonius wind turbines have several advantages over horizontal-axis wind turbines (HAWTs), such as low noise, low wind speed operation, and independence from wind direction. However, they also have lower aerodynamic efficiency and power output than HAWTs. Each turbine category has advantages and disadvantages over each other, as summarized in the Table 1.

NOMENCLATURE

A	turbine area	*T*	torque
BR	Blockage Ratio	*TKE*	Turbulance Kinetic Energy
C_p	power coefficient	*TSR*	Tip Speed Ratio
C_t	torque coefficient	*V*	wind velocity
D	rotor diameter	ω	angular velocity
R	moment arm	ρ	air density
RPM	Revolution Per Minute		

Table 1 Advantages and dis-advantages of VAWT and HAWT

Factors	VAWT	HAWT
Low production and installation costs	✓	
Durable and easy maintenance	✓	
Less noise	✓	
Independent from wind direction	✓	
Suitable for limited places	✓	
Relatively safer operation for avian	✓	
Scalable for larger wind farms		✓
Lower torque ripple		✓
Higher power efficiency		✓
Addition requirement in order to catch wind direction		✓

The design of a Savonius wind turbine can vary depending on the application and the desired performance. The classic barrel design consists of two half-cylinders that are slightly offset from each other on the shaft. The working principle of a Savonius wind turbine is based on the drag force that acts on the blades when they face the wind. The concave side of the blade experiences more drag than the convex side, creating a net torque that rotates the shaft. The performance metrics of the rotors are evaluated by computing the values of C_p and C_t representing the efficiency of power and torque of a rotor, respectively. Power and torque efficiencies are calculated as in Eqs. 1 and 2 respectively. For graphical representation, the non-dimensional values C_p and Ct are plotted against the tip speed ratio (TSR), which is defined by Equation 3.

$$C_p=\frac{T\omega}{\frac{1}{2}\rho(V)^3A} \quad (1)$$

$$C_t=\frac{T}{\frac{1}{2}\rho(V)^2AR} \quad (2)$$

$$\lambda=\frac{R\omega}{V} \quad (3)$$

Here, the (T) is the measured torque in N.m, (ω) is the angular velocity of the rotor shaft. Additionally, the wind velocity (V), air density (ρ), turbine area (A), and moment arm (R) are the other parameters that are used in above equations.

There are several augmentation techniques to enhance the rotor performances. Improvements can be realized by addition of external elements such as deflectors, wind curtains, and nozzles, rather than conducting any operations on the rotor blades. Alternatively, these enhancements can solely be achieved through modifications to the rotor blades. The aim is to enhance the positive pressure generated by focusing the wind on the concave section of the rotor, while simultaneously reducing the negative pressure formed in the convex section. Some of the blade design parameters that can affect the aerodynamic performance are the shape, size, stage number, overlap ratio, and twist angle of the blades. The study of Al-Ghriybah and Lagum (2023) suggested that adding quarter elliptical supplementary blades can improve the power coefficient by 13.1%, by enhancing the amount of captured wind and reducing the torque which is result of wind force acting on convex side of the rotor blade. Al-Faruk and Sharifian (2016) compared a classical Savonius rotor and their proposed swirling Savonius rotor in terms of power and torque efficiencies with series of experiments. The findings of their research indicated that the swirling rotor showed superior power coefficient performance against the conventional Savonius rotors. However, the researchers also noted that both swirling and conventional rotors show almost identical performance at lower angular velocities. Table 2 provides a summary of various studies available in the literature that relate to the enhancement of Savonius rotor blades.

Table 2 Studies conducted to enhance the Savonius rotor blades

Study	Type	Description of Design	Power Coefficient (C_p)
(Laws et al., 2020)	Numeric	Modified blade	Improved by 10 % - 28 %
(Lajnef et al., 2020)	Numeric	Delta blade	Improved by 14.5 %
(Al-Ghriybah & Lagum, 2023)	Numeric	Supplementary blades with quarter elliptical shapes	Improved by 13 %
(Sharma & Kumar, 2016)	Numeric	Multiple quarter plate	Improved by 9 % - 14 %
(Al-Faruk & Sharifian, 2016)	Experimental	Swirling blade	Improved by 24 %
(Sanusi et al., 2016)	Experimental	Combined blade	Improved by 11 %
(Saha & Rajkumar, 2006)	Experimental	Twisted blade	Improved by 14 %
Current Study	**Experimental**	**Optimized blade**	**Improved by 37.5%**

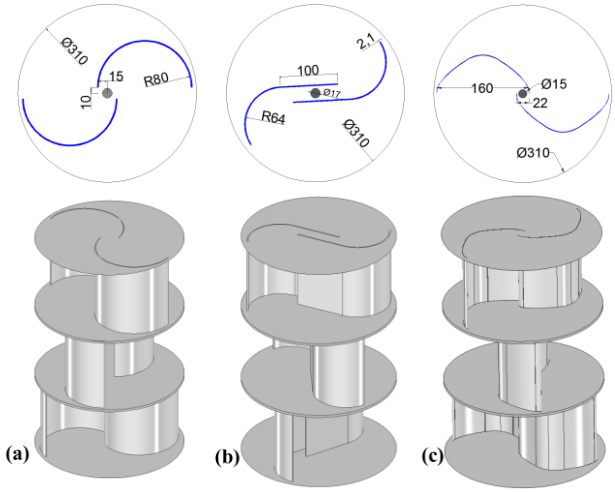

Fig. 1 A planar perspective of the traditional Savonius rotor (a), Banesh rotor (b) and Optimized rotor (c) employed in the numerical simulations. Note that all dimensions are in mm

This research described here focused on enhancing power efficiency (C_p) by optimizing the blade design of Savonius wind turbines. Then, the C_p value for a rotor employing the optimized blade is compared with the traditional and Banesh type Savonius rotors through numerical modelling and the results are presented.

2. METHODS

2.1 Attributes of the Rotors Employed in the Investigation

For this research, we utilized both the traditional three-stage Savonius rotor and the Banesh-style Savonius rotor, which also has three stages. The stages of both rotor types can be manipulated to achieve relative angles of 0º (all blades aligned) and with 60º phase difference between the stages. Characteristics of the rotors employed in the simulations are presented in Table 3. Furthermore, our novel design, featuring optimized turbine blades, was meticulously developed by applying the Ansys Adjoint Solver software (please see Section 2.2a for details). The performance of this optimized rotor was subsequently compared to that of the traditional and the Banesh style Savonius rotors. We used numerical modeling with Ansys Fluent software to conduct a comparative analysis focused on turbine performance. The details of the proposed design are given in Fig. 1.

2.2 Optimization of Turbine Blades for the New Rotor Design

The Ansys Fluent Adjoint Solver is an add-on that augments the functionality of Ansys Fluent, a widely-used computational fluid dynamics (CFD) software. This add-on is engineered to streamline shape optimization in an intelligent and automated fashion. The Adjoint Solver utilizes a distinctive sensitivity-based algorithm to refine existing designs and export the adjusted geometry. This attribute is especially advantageous in minimizing the time required for shape optimization. The solver interprets the objectives defined by the user and autonomously

Table 3 Characteristics of the rotors used in this study

Traditional Savonius rotor, Three-stages with 0° phase shift, S (0)	
Total rotor height (m)	0.5
Stage height (m)	0.5
Rotor width (m)	0.3
Aspect ratio	1.67
Number of stages	1
Blade diameter (m)	0.16 (see Fig. 1a)
Traditional Savonius rotor, Three-stages with 60° phase shift, S (60)	
Total rotor height (m)	0.5
Stage height (m)	0.17
Rotor width (m)	0.3
Aspect ratio	1.67
Number of stages	3
Blade diameter (m)	0.16 (see Fig. 1a)
Banesh Savonius rotor, Three-stages with 0º phase shift, B (0)	
Total rotor height (m)	0.5
Stage height (m)	0.5
Rotor width (m)	0.3
Aspect ratio	1.67
Number of stages	1
Blade diameter (m)	0.128 (see Fig. 1b)
Banesh Savonius rotor, Three-stages with 60º phase shift, B (60)	
Total rotor height (m)	0.5
Stage height (m)	0.17
Rotor width (m)	0.3
Aspect ratio	1.67
Number of stages	3
Blade diameter (m)	0.128 (see Fig. 1b)
Optimized blade Savonius rotor, Three-stages with 0º phase shift, OPT (0)	
Total rotor height (m)	0.5
Stage height (m)	0.5
Rotor width (m)	0.3
Aspect ratio	1.67
Number of stages	1
Blade diameter (m)	0.16 (see Fig. 1c)
Optimized blade Savonius rotor, Three-stages with 60º phase shift, OPT (60)	
Total rotor height (m)	0.5
Stage height (m)	0.17
Rotor width (m)	0.3
Aspect ratio	1.67
Number of stages	3
Blade diameter (m)	0.16 (see Fig. 1c)

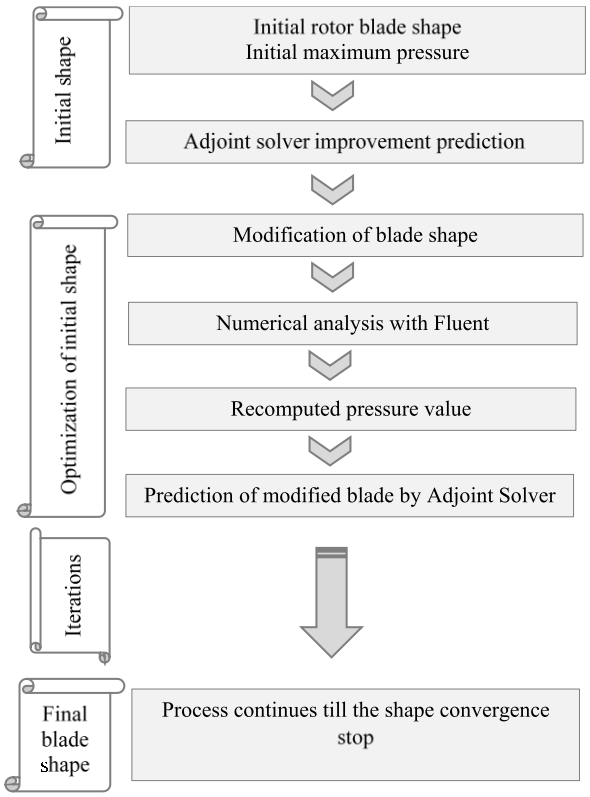

Fig. 2 Flow chart of the shape optimization analyses

morphs and optimizes the geometry. It is capable of identifying the most efficient shape and diminishing simulation duration (Ansys Fluent Gradient-Based Optimization, 2019; Ansys Fluent Adjoint Solver-based Optimization, 2019). Shape optimization steps with adjoint solver is shown in the flowchart below (Fig. 2).

In this particular application, the method of adjoint optimization was employed with the objective of amplifying the pressure force exerted on a semicircular structure with a diameter of 15 cm. In the context of the Gradient-Based Optimizer, the 'shape-opt' has been chosen as the shape optimizer type. The objectives of the analysis have been configured to utilize a step size of 10. As for the optimizer settings, the 'adaptive-step-size' method has been selected. The number of design iterations and flow iterations have been set at 10 and 300, respectively. The convergence criteria have been established at 0.01, and the number of Adjoint iterations has been inputted as 300. In the Mesh Quality segment, the minimum orthogonal quality has been designated as 0.01. In the Post Morph section, the smoothing option has been chosen.

Subsequent to the computational analysis, the total pressure acting upon the surface of the initial configuration was determined to be 37630 Pa. Using a 10% pressure increase per iteration, we reached convergence at the 34th step with a pressure of 597800 Pa, about 16 times greater than the initial value. To confirm the initial result, total pressure was increased by 15% per iteration until convergence at the 16th step. The calculated total pressure was 609400 Pa which is 16.2 times greater than the initial value. The transition of the rotor blade design from a semi-circular form to the newly proposed design is given together with the pressure distributions simulated on the blade surface before and after the optimization process (Fig. 3).

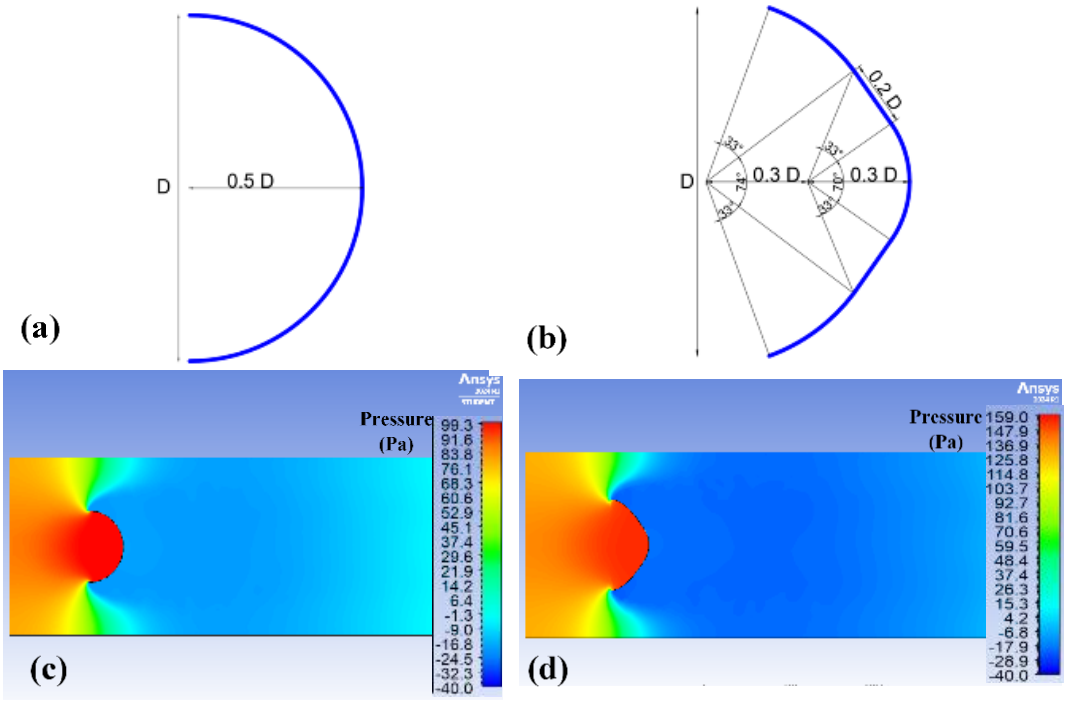

Fig. 3 Blade shapes at the beginning of the optimization (initial shape) (a), and at the end of the optimization process (b). Maximum pressure distributions at the beginning of the optimization (c) and at the end of the optimization process (d)

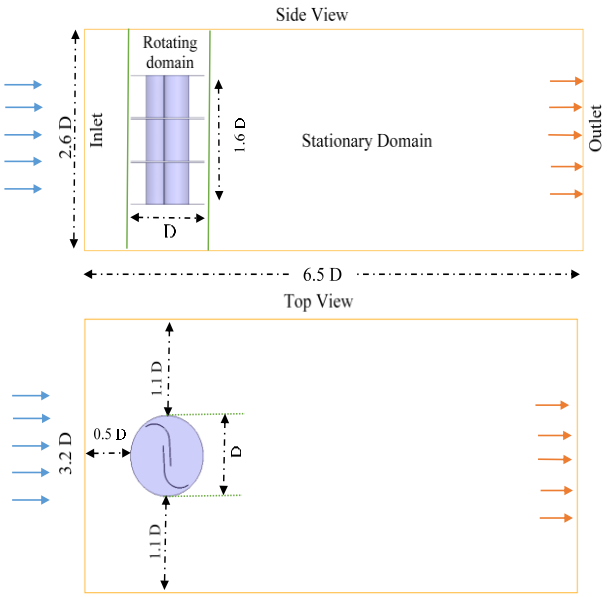

Fig.4 Details of the model domain

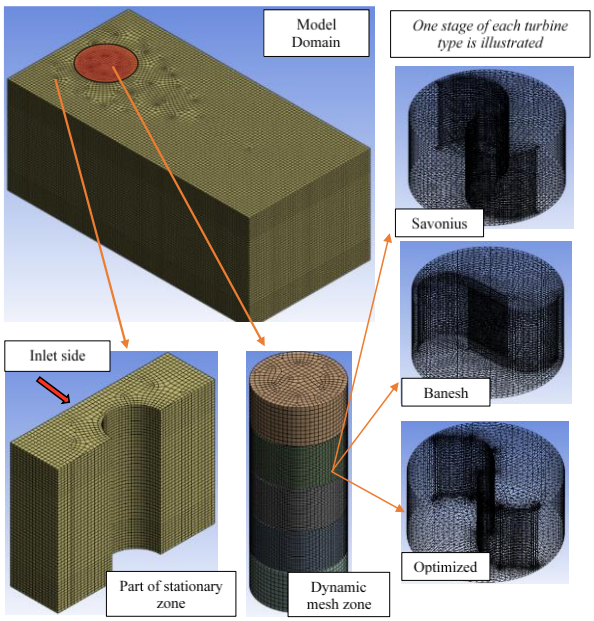

Fig. 5 Details of the mesh zones of the model domain

2.3 Numerical Simulations of Savonius Rotors Employing Ansys Fluent Software

The Ansys Fluent software was employed to conduct numerical modeling of rotor performance, when deployed in a simulated flume. In the model, the rotor and the flume were defined as distinct entities. The model domain consists of rotor, flume, inlet, outlet, and stationary wall sections as shown in Fig. 4. The surfaces of the flume, excluding the inlet and outlet, are characterized as stationary walls. The dynamic mesh is a sophisticated instrument utilized when the model's domain experiences time-dependent changes due to its inherent motion and it can simulate the complex dynamics and behaviors of fluid flow. In this simulation, as the Savonius rotor rotates within the airflow, its rotational motion impacts the surrounding mesh. Consequently, a dynamic mesh is employed to accurately represent the changes as the rotor rotates. To effectively apply the dynamic mesh technique, a cylinder encompassing the entire rotor width and representing the moving (rotating) part which is shown in Fig. 5 has been defined. The outer surfaces of the rotor and the surrounding cylinder were designated as a rigid body to define the dynamic mesh region. The remainder of the model domain, excluding these dynamically meshed sections, was defined as stationary. Additionally, the Dynamic Mesh 6DOF method, which simulates turbine motion based on moment forces, was chosen for the analysis.

Mesh independence testing was carried out to determine the most suitable mesh size for accurate and efficient simulations by evaluating parameters like velocity, pressure, and turbulence energy. The process involved refining the mesh through multiple levels until the results stabilized and showed minimal differences. A specific mesh size was chosen as it provided reliable outcomes while balancing accuracy and computational efficiency. Figure 6 demonstrates how key parameters became steady as the mesh was refined, confirming the selected size for further analysis.

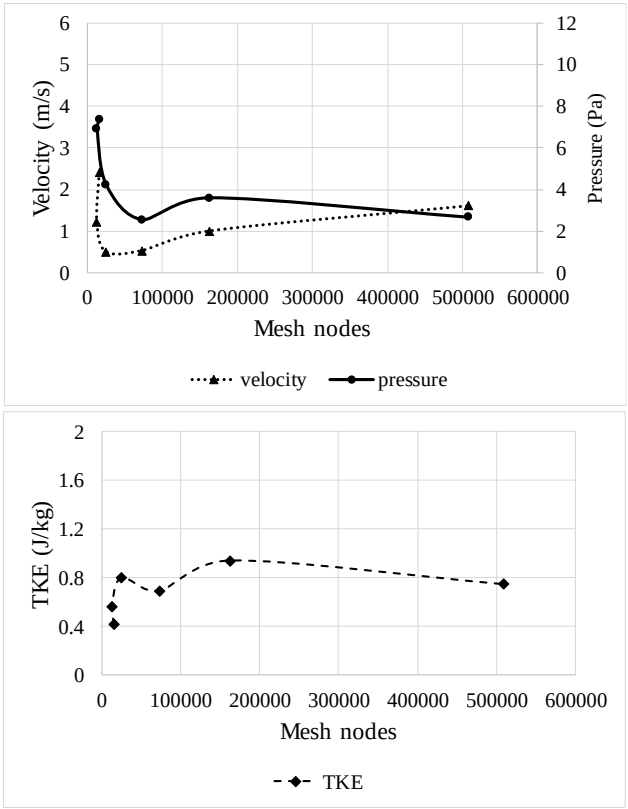

Fig. 6 Mesh independence testing of velocities, pressures and turbulent kinetic energies for various numbers of elements

The rotor segment within the dynamic mesh zone underwent a detailed meshing process, while the remaining parts of the solution domain were meshed with a larger size to enhance analysis efficiency. The quality of the meshes generated within the numerical model was assessed by considering parameters such as skewness, orthogonal quality, and aspect ratio values. To ensure

Table 4. Mesh quality parameters

Rotor Type	Average Skewnees	Average Orthogonal Quality	Average Aspect Ratio
S (0)	0.0076	0.938	1.731
S (60)	0.0067	0.946	1.754
B (0)	0.0052	0.965	1.606
B (60)	0.0058	0.955	1.674
OPT (0)	0.1160	0.8934	2.383
OPT (60)	0.1139	0.8923	2.252

optimal mesh quality, it is desirable for skewness values to approach zero, while the orthogonal quality should ideally trend towards one (Elçi et al., 2023). Additionally, it is recommended that to keep aspect ratio smaller than 5. Summary of the mesh quality parameters for all rotor types are shown in Table 4.

In this study, the k- ε realizable model was chosen for the simulation of the Savonius rotor. We used scalable wall functions in conjunction with the k-ε realizable model to ensure accuracy, particularly in areas where turbulence near the wall is critical. The k-ε realizable model was selected over other turbulence models due to its superior performance in flows involving rotation, boundary layers with strong adverse pressure gradients, separation, and recirculation, as documented in the Fluent model manual (ANSYS, 2018). The Semi-Implicit Method for Pressure-Linked Equations (SIMPLE) algorithm, a renowned pressure-velocity coupling method in the realm of Computational Fluid Dynamics, is chosen as the solution methodology. This algorithm, which provides a numerical solution to the Navier-Stokes equations, is paired with a second-order upwind scheme for all spatial discretization options to ensure the precision of the results.

The mass and momentum conservation equations are fundamental for governing flow for CFD modelling. These governing equations for incompressible, unsteady, and viscous flow for mass and momentum are given in Eqs. 4 and 5 respectively.

$$\frac{\partial \rho}{\partial t}+\frac{\partial(\rho u_i)}{\partial x_i}=0 \tag{4}$$

$$\rho \frac{Du_i}{Dt}=\rho\left(\frac{\partial u_i}{\partial t}+u_j\frac{\partial u_i}{\partial x_j}\right)=\rho f_i-\frac{\partial P}{\partial x_i}+\mu\frac{\partial^2 u_i}{\partial x_j \partial x_i} \tag{5}$$

The domain of the model is defined by dimensions of 3.2D in width, 2.6D in height, and 6.5D in length. Here, "D" denotes the diameter of the Savonius rotor, which is precisely 0.31 meters. Therefore, the actual dimensions of the model domain correspond to 1 meters in width, 0.8 meters in height, and 2 meters in length. As shown in Fig. 4, the model domain is configured as follows: The left boundary is designated as a velocity inlet, characterized by a constant air velocity of 4 m/s and a constant density of 1.225 kg/m³. The right boundary is defined as a pressure outlet. All other boundaries, including the top, bottom, and side walls (excluding the aforementioned inlet and outlet), are specified as stationary walls. This configuration ensures a precise simulation of the physical scenario under consideration. The simulation is configured with a time step of 0.01 seconds, and it runs for a total of 20,000 time steps. This duration, equivalent to 200 seconds, represents the minimum time necessary for a rotor to achieve its maximum and steady revolutions per minute (RPM)

Table 5. Boundary conditions and model parameters used in the simulations

Boundary	Definition	Magnitude/Value
Inlet	velocity	4 m/s uniform
Outlet	pressure	1 atm
Bottom, top and side walls	stationary wall	

Model Setup	Magnitude/Value
Air density	1.225 kg/m^3
Air velocity	4 m/s
Turbulent model	k-ϵ realizable
Pressure-velocity coupling	SIMPLE algortihm
Time step size	0.01 sec

condition. This setup ensures an accurate representation of the rotor's operational characteristics. Details of the boundary conditions and numerical model setup is given in Table 5.

3. Results and Discussion

3.1 Investigation of Blockage Ratio on Rotor Performance

The numerical model domain includes a rotating Savonius rotor and an outer volume, similar to testing a Savonius rotor in a wind tunnel. However, because the wind tunnel or model domain is geometrically limited, the testing conditions are not exactly like those in the open atmosphere. Consequently, the blockage ratio, denoted as BR (the ratio of the rotor's area to the test section's area), emerges as a crucial element in rectifying the outcomes of both numerical modelling and experimental investigations conducted within closed test domain. It has been suggested that, under optimal conditions, the blockage ratio for a model should not exceed 5% (Chen & Liou, 2011).

The width dimension was chosen after several trials with different values, aiming to reduce the blockage effect. As illustrated in the Fig. 7, a flume width corresponding to a blockage ratio (BR) of 0.375, results in a C_p value exceeding 0.4 for Banesh (60) type rotor. However, BR of 0.188 results decrease in the C_p value to just above 0.35. We found that once the blockage ratio was below 0.19, it had negligible impact on C_p. Based on our analyses, the minimum width that effectively eliminates the blockage effect has been identified as 1 meter for the current simulations. Any further increase beyond this value does

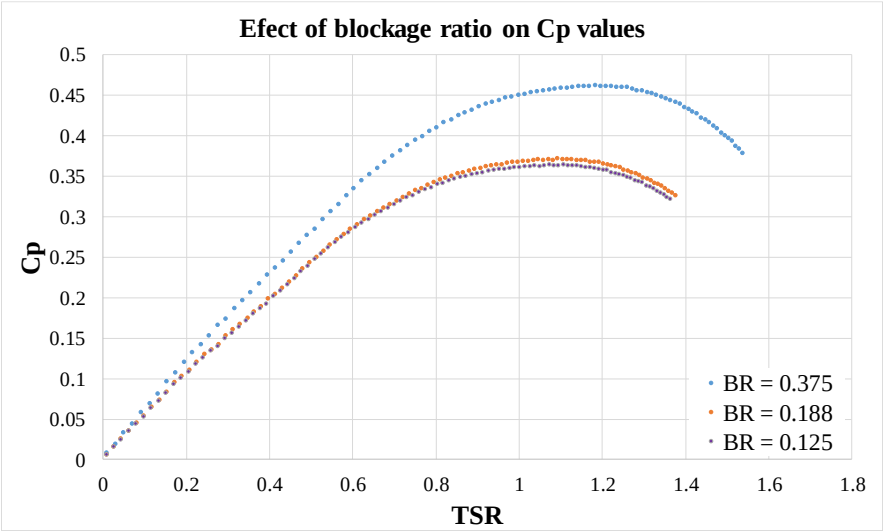

Fig. 7 Examining the impact of the blockage ratio on the power coefficient using Banesh (60) rotor.

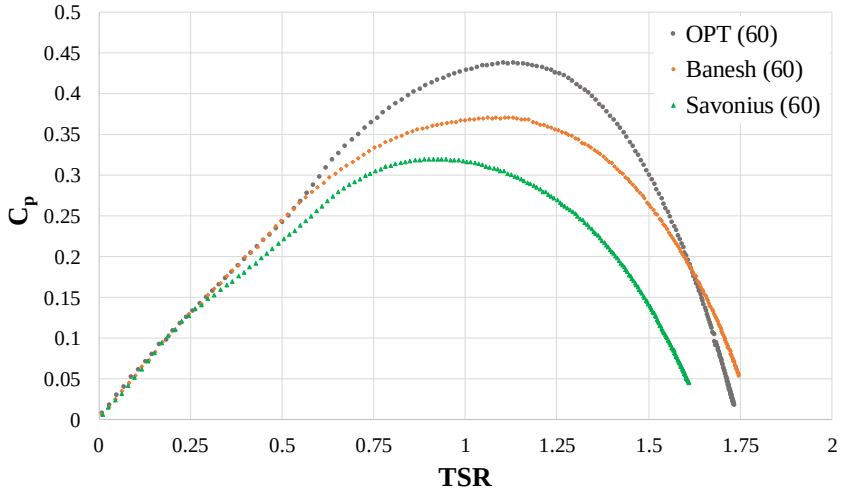

Fig. 8 Comparison of power efficiencies (C_p) of different rotors

not significantly impact the blockage effect, but it does contribute to an increase in computation time.

3.2 Evaluation of Rotor Performances

The performance of rotors is assessed by calculating the power coefficient (C_p) and torque coefficient (C_t) in relation to the tip speed ratio (TSR) as described earlier. The power and torque values are averaged for 1 second time interval. The analyses were conducted using various types of rotors, including classical Savonius rotors (3S(0) and 3S(60)), Banesh type Savonius rotors (B(0) and 3B(60)), and optimized rotors (OPT(0) and OPT(60)).

As illustrated in the Fig. 8 below, our novel rotor design, characterized by a shift angle of 60°, achieves the highest efficiency. This rotor yields a peak power coefficient of 0.44 at a rotational speed of 288 RPM, corresponding to a Tip Speed Ratio (TSR) of 1.13. Following our novel design, B(60) rotor exhibits the second highest efficiency values. Specifically, the B(60) rotor generates a maximum power coefficient of 0.37 at 276 RPM, equating to a TSR of 1.08. S(60) rotor exhibits the worst performance with maximum power coefficient of 0.32 at 229 RPM, corresponds to TSR of 0.9. The differences observed in the C_p values of the classical Savonius, Banesh-type Savonius, and our optimized blade design Savonius rotors for TSR values beyond 0.25 can be attributed to the distinct geometric design characteristics of these rotor types. Specifically, the superior performance of our turbine with its optimized blade structure, even at low TSR values, can be attributed to its specialized blade design. This unique configuration enables it to achieve high efficiency under a range of operating conditions.

Figure 9 provides a comparative analysis of torque efficiency across different rotor types. A preliminary review of the figure reveals the C_p values of the rotors varies within a Tip Speed Ratio (TSR) range of 0 to 0.25. In the time interval of 0.25 and 0.5, the B(60) and OPT(60) rotors demonstrate torque efficiencies that are closely matched, while the 3S(60) rotor exhibits the lowest efficiency. Beyond a Tip Speed Ratio (TSR) of 0.5, the

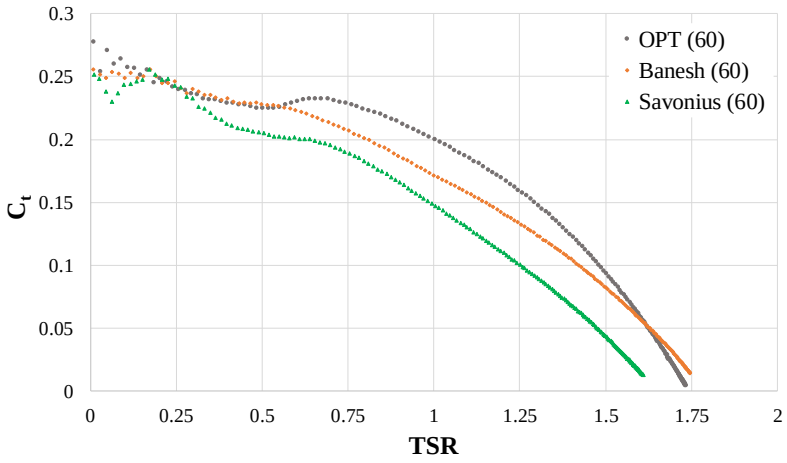

Fig. 9 Comparison of torque efficiencies (Ct) of different rotors

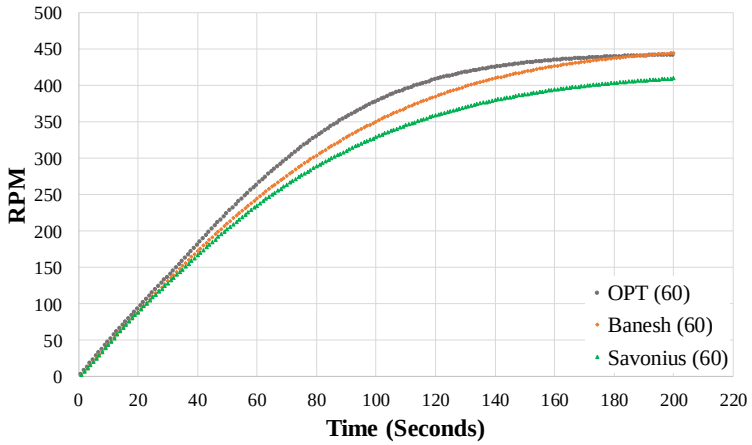

Fig. 10 Variation of the revolution of different rotors with time

novel rotor design begins to exhibit the highest C_t values. This new design maintains superior efficiency up to a TSR value nearing 1.6. Within this range, the B(60) rotor is the second most efficient rotor and the S(60) rotor yielded the lowest results. The superior torque performance of the OPT (60) rotor across a broad range of TSR values can be attributed to the aerodynamic blade design of our optimized rotor. This advanced design minimizes the negative pressure and torque on the returning blade, enhancing overall efficiency. However, beyond a TSR of 1.5, the efficiencies of OPT (60) and B (60) rotors converge.

Figure 10 presents a temporal analysis of the Revolutions Per Minute (RPM) values for various rotor types. It is observed that all rotor types approach a steady state around the 200-second mark. A comparative study of the acceleration patterns reveals a distinct behavior for our optimized rotor design as opposed to the other rotor types. The latter exhibit a consistent acceleration pattern from the commencement to the conclusion of the numerical simulation. Our optimized design, however, demonstrates an elevated acceleration post the 40-second mark. This heightened acceleration persists for the duration between 40 and 160 seconds, during which it registers superior RPM values. Furthermore, Fig. 10 illustrates that the enhanced acceleration rate of our optimized rotor design can be attributed to its advanced blade structure and superior aerodynamic design. After 200 seconds the RPM values of the rotors reach steady state condition. Table 6 summarizes numerical analysis results of all rotors.

When we examine the pressure distribution one centimeter behind the rotors, it's clear that the pressure values behind the advancing blade are relatively lower for the optimized rotor (Fig. 11). Additionally, there's a significant difference in the pressures on the returning and

Table 6 Summary of the numerical analysis results

Rotor Type	Max. C_p	Max. C_t
OPT (60)	0.44	0.28
OPT (0)	0.34	0.29
B (60)	0.37	0.26
B (0)	0.38	0.39
S (60)	0.32	0.26
S (0)	0.33	0.32

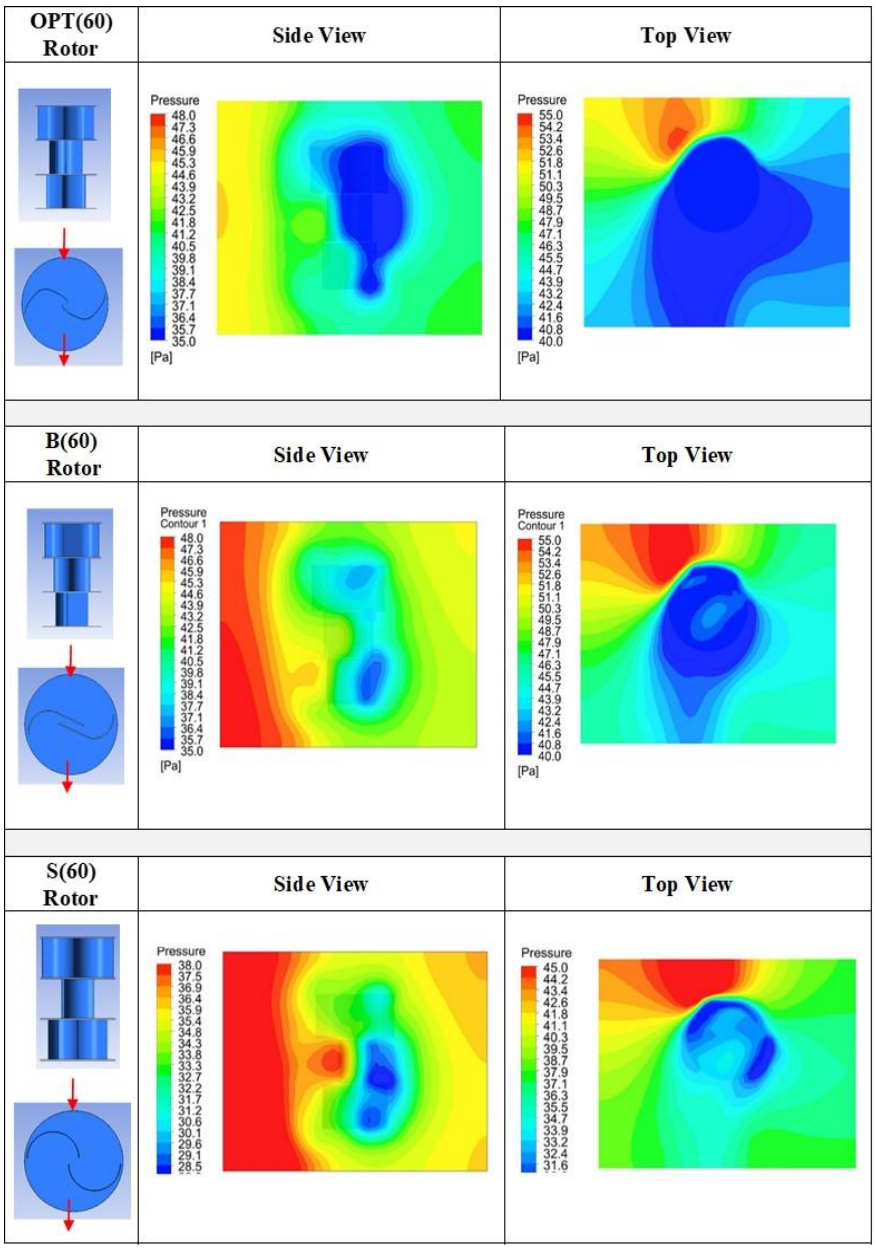

Fig. 11 Comparison of pressure variation (red arrows indicates the flow direction)

advancing blades. This situation further substantiates the superior performance of the optimized design rotor compared to other rotors, particularly in terms of C_p and C_t values.

On the other hand, when we examine the traditional Savonius rotor, it's evident that the pressure difference between the advancing and returning blades is relatively low. This can also be associated with the subpar performance of the rotor efficiency.

When we compare the velocity one cm behind the rotors, since the rotor diameters and stage phase angles are identical, there isn't a significant difference in air velocity (Fig. 12). However, there is a significant difference in terms of turbulent kinetic energy (Fig. 13). The TKE values behind the returning blade of the optimized rotor are greater than those of the other rotors. The lowest TKE values are observed in the Banesh type rotor. Figs 11, 12, and 13 present comparison of pressure, velocity and turbulence kinetic energy variations at the end of 200 seconds simulated at one cm behind the rotors, respectively.

In summary Figs 11, 12, and 13 collectively illustrate the interactions among pressure, velocity, and TKE. The optimized rotor demonstrates superior aerodynamic performance, with a pronounced pressure difference between the advancing and returning blades, correlating with higher C_p and C_t values (Fig. 11). In contrast, the traditional Savonius rotor shows minimal pressure variation, reflecting its lower efficiency. While velocity contours (Fig. 12) reveal no significant differences due to identical rotor diameters and phase angles, turbulent kinetic energy (TKE) contours (Fig. 13) reveal greater TKE behind the returning blade of the optimized rotor, signifying more efficient energy transfer. The Banesh-type rotor, with the lowest TKE values, demonstrates the least effective performance.

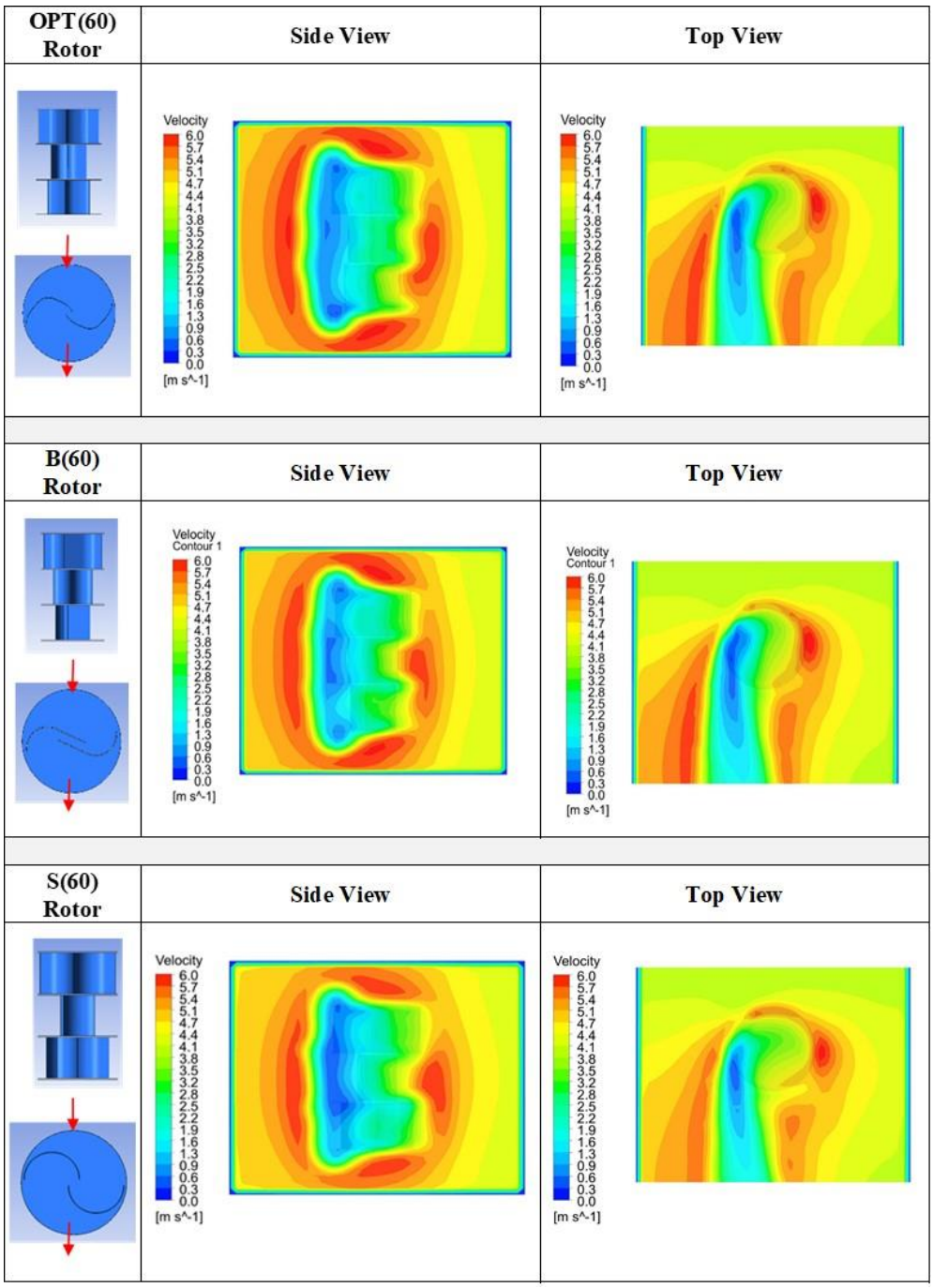

Fig. 12 Comparison of velocity variation (red arrows indicates the flow direction)

3.3 Investigating the impact of the number of stages on the optimized rotor performance

The numerical model results suggest that the OPT (60) rotor demonstrates superior power efficiency compared to the OPT (0) rotor (Fig. 14). The maximum C_p value for the OPT (60) rotor is 0.44, achieved at a TSR value of 1.13. In contrast, the OPT (0) rotor reaches its maximum C_p value of 0.34 at a TSR of 1.25. The variation in C_p values is quite pronounced between the TSR values of 0.5 and 1.5, with the OPT (60) rotor outperforming. However, as the TSR value goes beyond 1.5, the power efficiencies of both turbines start to align more closely and the OPT(0) rotor shows better results for very narrow TSR band.

Upon examining the torque efficiencies of these rotors (Fig. 15), it's clear that the torque efficiency of the OPT (0) rotor varies greatly during the TSR range from 0 to 0.5. Over this range, the OPT (60) rotor displays more consistent results and generally exhibits higher C_t values. Between the TSR of 0.5 and 1.375, the OPT (60) rotor clearly outperforms in terms of C_t value. However, when the TSR exceeds 1.375, the OPT (0) rotor achieves higher C_t values for a limited TSR band.

As demonstrated by both the power and torque efficiency measures, the performance of the rotor is considerably more efficient when the total height of the turbine is held constant and three stages are established, each with a phase angle of 60°.

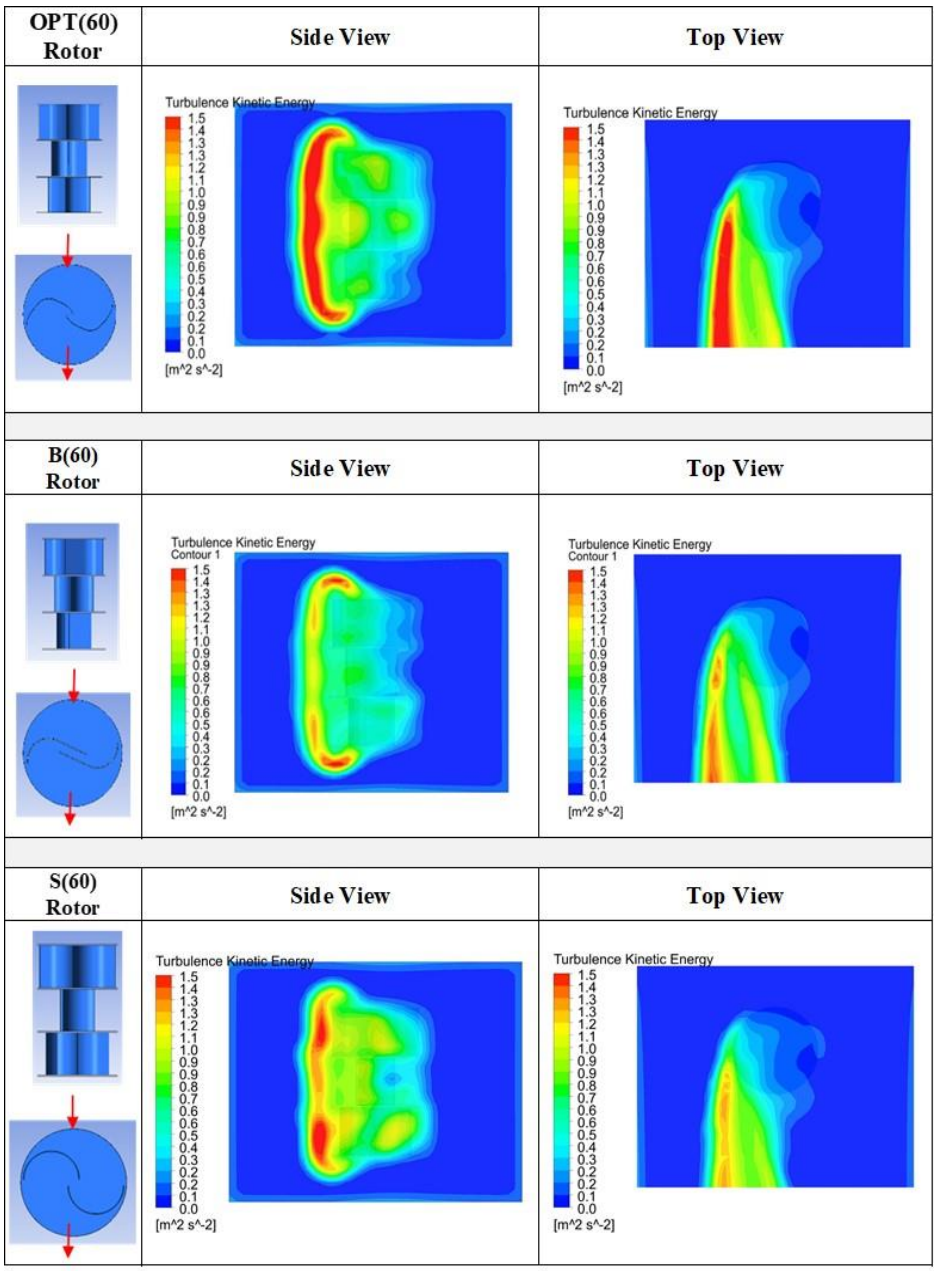

Fig. 13 Comparison of turbulence kinetic energy variation (red arrows indicates the flow direction)

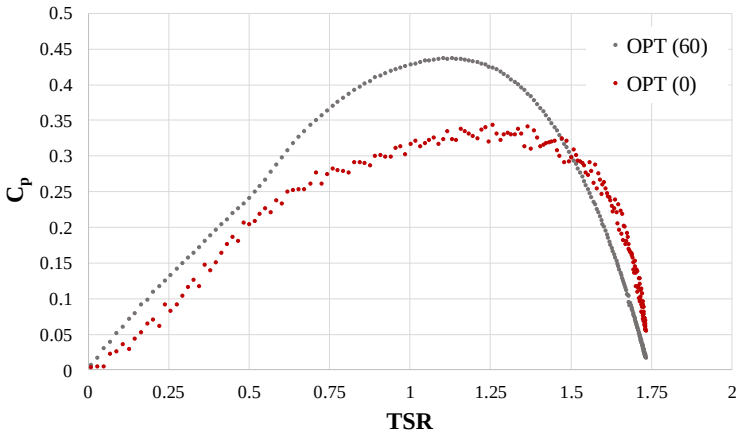

Fig. 14 Effect of stage number on C_p performance of optimized rotor

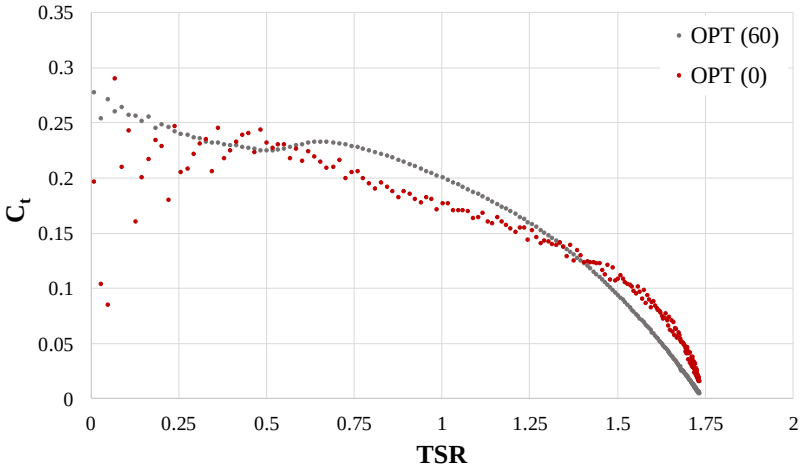

Fig. 15 Effect of stage number on C_t performance of optimized rotor

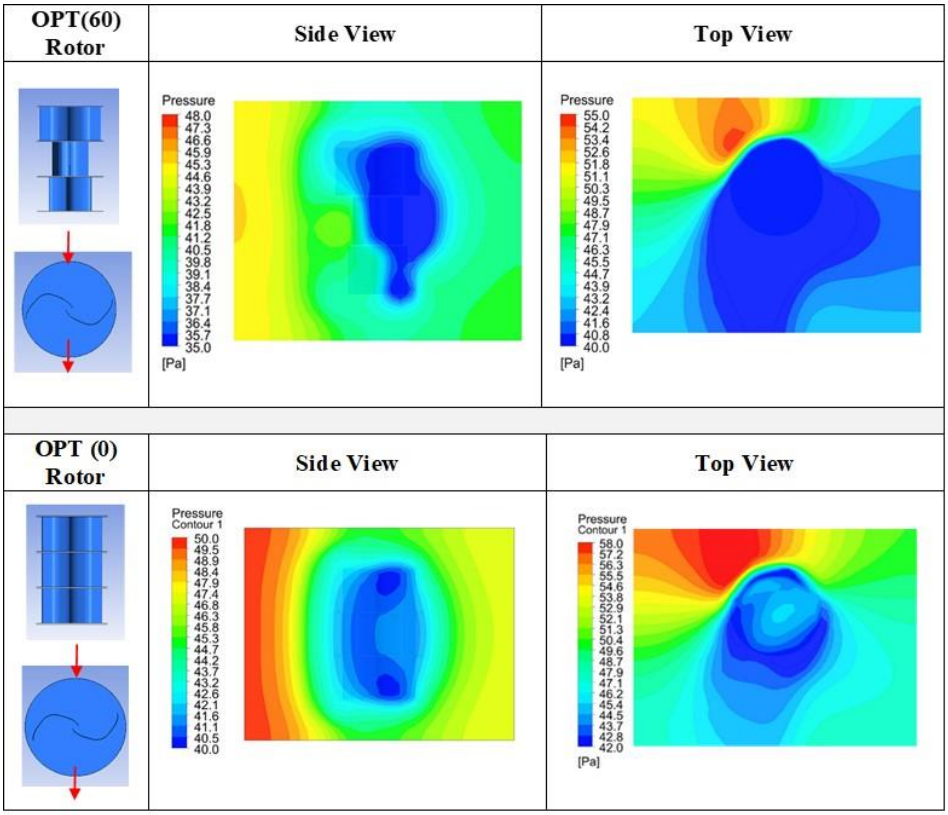

Fig. 16 Comparison of pressure variation at steady state one cm behind the OPT (60) and OPT (0) rotors

Figure 16 indicates that the OPT (60) rotor exhibits a slightly larger pressure difference between the advancing and returning blades compared to the OPT (0) rotor. This physical characteristic is one of the key factors that contribute to the superior performance of the OPT (60) rotor over the OPT (0) rotor.

In agreement with Fig. 16, Fig. 17 indicates that the OPT (60) rotor exhibits slightly smaller velocity difference between the advancing and returning blades compared to the OPT (0) rotor. Figure 18 shows that TKE is close to each other but TKE of OPT (60) rotor is slightly higher than the OPT (0) rotor.

3.4 Comparison of the Fluctuations in Dynamic Torque

Figure 19 illustrates the moment fluctuations of each rotor under steady-state conditions. It is evident from the figure that the optimized design Banesh type and traditional Savonius rotors, characterized by a shift angle of 60°, exhibit more stable moment values compared to rotor types with a 0° shift angle. These results suggest that multiple stages, each equipped with two blades, can function in parallel, thereby diminishing moment fluctuations. These results are also in agreement with those of Saha et al (2008) and Hayashi et al (2005) where they had suggested using multiple stages to reduce

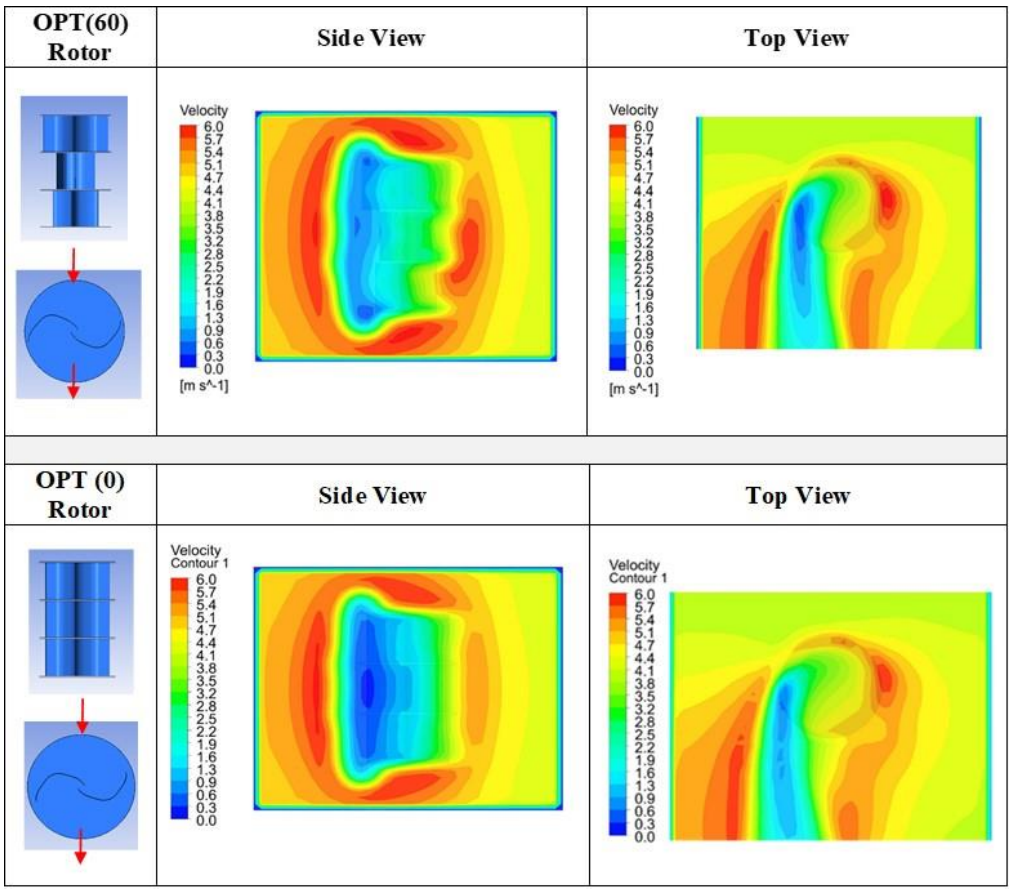

Fig. 17 Comparison of velocity variation at steady state one cm behind the OPT (60) and OPT (0) rotors

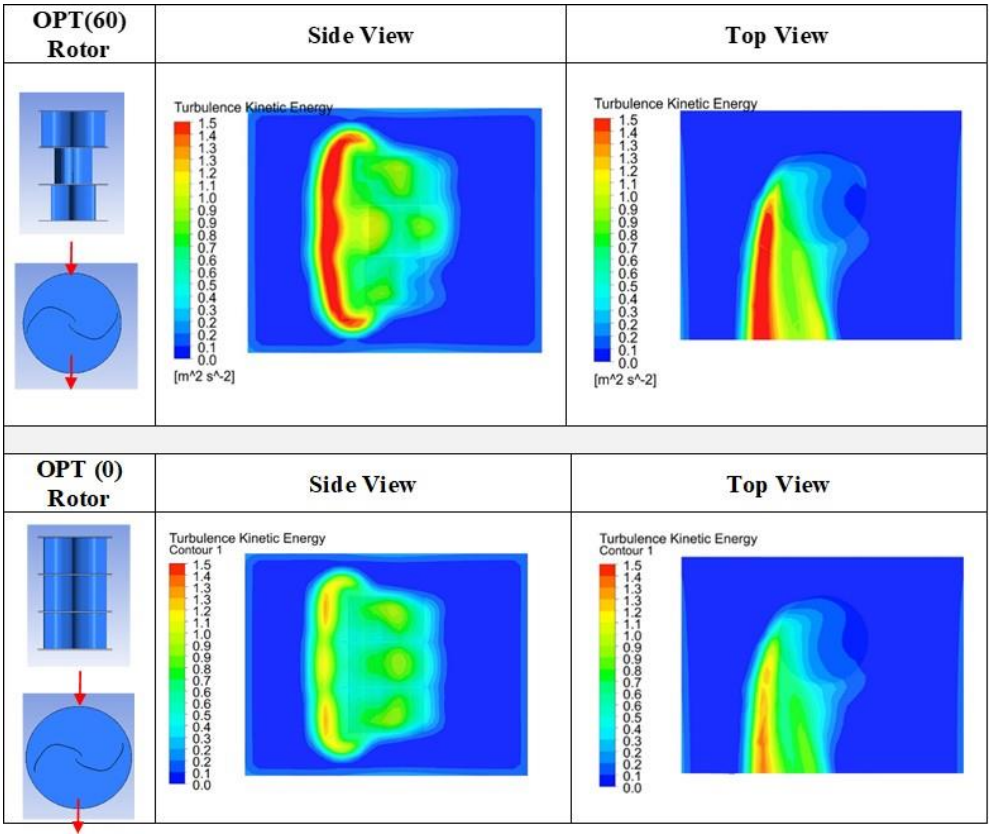

Fig. 18 Comparison of turbulence kinetic energy variation at steady state one cm behind the OPT (60) and OPT (0) rotors

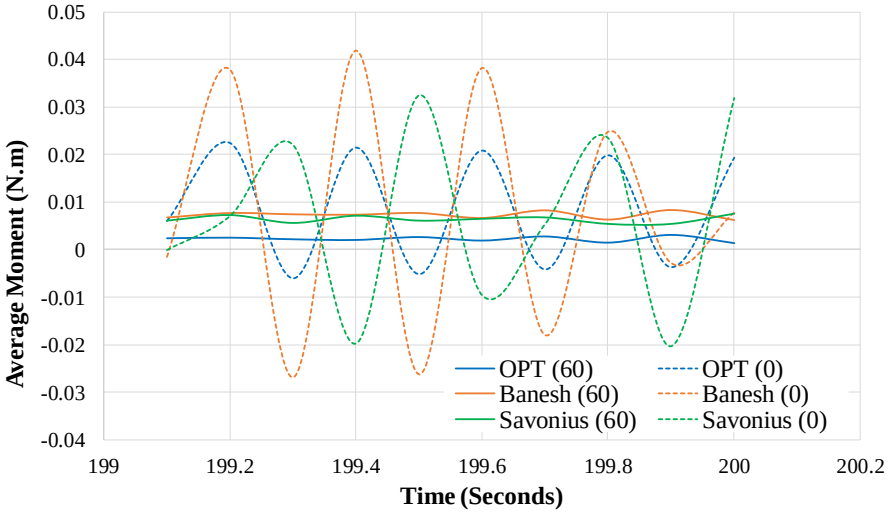

Fig. 19 Moment fluctuations for each rotor with time

moment fluctuations, without significant performance loss. This approach entails the transmission of power to the rotor shaft and the operation of cycles that are staggered relative to each other.

4. CONCLUSION

The study described here featured a numerical analysis of three unique Savonius rotors: the traditional Savonius, the Banesh-type Savonius, and the Optimized Savonius. The blade shape of the Optimized Savonius is determined through analyses using the ANSYS adjoint solver optimization. The performance of the rotors was evaluated under a constant wind velocity of 4 m/s, focusing on power and torque coefficients. The numerical analyses were carried out using ANSYS Fluent software. The Semi-Implicit Method for Pressure Linked Equations (SIMPLE) was employed alongside the SST k-ϵ turbulence model during the analyses. A dynamic mesh was utilized to simulate realistic turbine rotation. As a result, graphs of power and torque coefficients in relation to TSR were plotted. The flow around the rotors was visualized by examining pressure, velocity, and turbulence kinetic energy plots for all rotors.

The presented study yielded the following conclusions.

- The results show that the stage phase angle which is the relative position of rotor blades from one stage to another, has a significant impact on the efficiency of optimized rotor. Optimized rotor with three stages (phase angle of 60º) demonstrates superior efficiency compared to the optimized rotor with single stage (phase angle of 0º). As for the traditional and Banesh type Savonius rotors, having multiple stages did not yield to a significant efficiency improvement over the single stage rotors.

- While maintaining the same overall rotor height, moment fluctuations in the rotation of the blades can be significantly reduced by replacing the single-stage rotor (0º phase angle) with a three-stage rotor (60º phase angle) in all rotor types.

- Shape optimization enhance the pressure on the advancing rotor blade while minimizing the pressure on the returning blade and significantly increase the rotor performance.

- The optimized rotor OPT(60) in this study, exhibits greater power efficiency (C_p) compared to B(60) and S(60) rotors. Its C_p value is 18.9% and 37.5% higher than the Banesh-type Savonius and traditional Savonius rotors, respectively, indicating a significant improvement in rotor efficiency.

- The OPT (60) rotor proved to be more efficient than the OPT (0) rotor, achieving a maximum power coefficient (Cp) of 0.44, whereas the OPT(0) rotor reached a maximum Cp of only 0.34.

ACKNOWLEDGEMENTS

This study was funded by a research by a grant from The Scientific and Technological Research Council of Turkey (TUBITAK) through Project No: 122M849.

We would like to express our gratitude to Dr. Paul Work, visiting IZTECH as guest researcher under the Fulbright program, for his valuable proofreading and comments.

CONFLICT OF INTEREST

The authors declare no conflicts of interest.

AUTHORS CONTRIBUTION

Oğuz Hazar: Conceptualization, Writing-Original draft preparation, Methodology, Formal Analysis. **Şebnem Elçi:** Conceptualization, Methodology, Writing-Reviewing and Editing, Supervision. **Mehmet Dirgenali:** Formal Analysis. **Karahan Kaçar:** Formal Analysis.

REFERENCES

Al-Faruk, A., & Sharifian, A. (2016). Geometrical optimization of a swirling Savonius wind turbine using an open jet wind tunnel. *Alexandria Engineering Journal, 55(3),* 2055-2064. https://doi.org/10.1016/j.aej.2016.07.005

Al-Ghriybah, M., & Lagum, A. A. (2023). Enhancing the aerodynamic performance of the Savonius wind turbine by utilizing quarter elliptical supplementary blades. Flow, *Turbulence and Combustion, 112(3),* 491-508. https://doi.org/10.1007/s10494-023-00516-0

ANSYS Fluent User's Guide, (2019) R1a, Section on 'Ansys Fluent Adjoint Solver-based Optimization'.

ANSYS Fluent User's Guide, (2019) R1b, Section on 'Ansys Fluent Gradient-Based Optimization'.

ANSYS Inc. ANSYS Fluent Tutorial Guide R18; ANSYS Inc.: Canonsburg, PA, USA, (2018*).*

Chen, T. Y., & Liou, L. R. (2011). Blockage corrections in wind tunnel tests of small horizontal-axis wind turbines. *Experimental Thermal and Fluid Science, 35(3),* 565-569. https://doi.org/10.1016/j.expthermflusci.2010.12.005

Elçi, Ş., Hazar, O., Bahadıroğlu, N., Karakaya, D., & Bor, A. (2023). Destratification of thermally stratified water columns by air diffusers. *Journal of Hydro-Environment Research, 46,* 44-59. https://doi.org/10.1016/j.jher.2022.12.001

Giovanni, S. (2019). *Wind science and engineering: Origins, developments, fundamentals and advancements*. Springer. ISBN 9783030188153. https://doi.org/10.1007/978-3-030-18815-3

Hayashi, T., Li, Y., & Hara, Y. (2005). Wind tunnel tests on a different phase three-stage Savonius rotor. *JSME International Journal Series B: Fluids and Thermal Engineering, 48*(1), 9-16. https://doi.org/https://doi.org/10.1299/jsmeb.48.9

IEA (2024), Renewables 2024, IEA, Paris https://www.iea.org/reports/renewables-2024, Licence: CC BY 4.0

IRENA (2019). Future of wind: Deployment, investment, technology, grid integration and socio-economic aspects (A Global Energy Transformation paper). International Renewable Energy Agency, Abu Dhabi. ISBN 978-92-9260-155-3.

Lajnef, M., Mosbahi, M., Chouaibi, Y., & Driss, Z. (2020). Performance improvement in a helical Savonius wind rotor. *Arabian Journal for Science and Engineering, 45(9),* 9305-9323. https://doi.org/10.1007/s13369-020-04770-6

Laws, P., Saini, J., Kumar, A., & Mitra, S. (2020). Improvement in Savonius wind turbines efficiency by modification of blade designs—A numerical study. *Journal of Energy Resources Technology, 142(6),* 061303. https://doi.org/10.1115/1.4045476

Saha, U. K., & Rajkumar, M. J. (2006). On the performance analysis of Savonius rotor with twisted blades. *Renewable Energy, 31(11),* 1776-1788. https://doi.org/10.1016/j.renene.2005.08.030

Saha, U. K., Thotla, S., & Maity, D. (2008). Optimum design configuration of Savonius rotor through wind tunnel experiments. *Journal of Wind Engineering and Industrial Aerodynamics, 96(8–9),* 1359-1375. https://doi.org/10.1016/j.jweia.2008.03.005

Sanusi, A., Soeparman, S., Wahyudi, S., & Yuliati, L. (2016). Experimental study of combined blade Savonius wind turbine. *International Journal of Renewable Energy Research, 6(2).* https://doi.org/10.20508/ijrer.v6i2.3455.g6826

Sharma, S., & Kumar, S. R. (2016). Performance improvement of Savonius rotor using multiple quarter blades – A CFD investigation. *Energy Conversion and Management, 127,* 43-54. https://doi.org/10.1016/j.enconman.2016.08.087